Reports in Mechanical Engineering
Vol. 6, No. 1, 2025, pp. 55-73
ISSN: 2683-5894, DOI: https://doi.org/10.31181/rme448

Butt Joining of Aluminum Sheets Using Face Filler Friction Stir Spot Welding

Isam Tareq Abdullah, Mohanad Kadhim Mejbel*
Middle Technical University, Technical Engineering College-Baghdad, 10074 Baghdad, Iraq

Article Info

Article history:

Received June 12, 2025
Revised July 15, 2025
Accepted August 19, 2025

Keywords:
Butt Joining,
Friction,
Manufacturing Process,
Aluminum Alloy,
Face Filler

ABSTRACT

Friction stir spot welding FSSW, as a general rule, is adopted and limited for joining sheets of similar or dissimilar metals in a lap joint configuration, and it cannot be used in butt jointsss. The idea of this study is to weld two AA 1050 aluminum sheets in a butt joint configuration, having a thickness of 2 mm each, by using a face filler disk from the same AA 1050 alloy of 1 mm thickness via friction stir spot welding. A stir tool (rod or welding tool) is made from HSS high-speed steel. A special fixture is manufactured to hold and weld the sheets with the facial filling in a butt configuration. Three different rotational speeds (1120, 1400, and 1800 revolutions per minute) with a linear movement in a direction perpendicular to the facial filling and then to the sheets were used. The samples were welded with and without preheating, with the stirring tool lowered by 1 mm in a vertical orientation. The best result obtained regarding the force applied to break the welded sample is 4000 Newtons as a tensile force, with a joint efficiency of 72% compared to the strength of the original metal. Also, we obtained a tensile strength to break the welded joint of 125 MPa compared to the tensile strength of the original metal, with a joint efficiency of 113% of the tensile strength of the original metal. The cross-sectional area of the fracture was also observed, which was acceptable from the point of view of microscopic examination. No traces of the contact area between the two sheets were seen, and the fusion of the two sheets was perfect. With the elimination of the keyhole, considered a flaw in the standard friction stir spot welding procedure, it was possible to obtain keyhole-less areas while maintaining adequate joint strength. The metallurgical bonding between the face filler disc and the lower sheet causes the disc to become a part of the spot when inserted into the lower sheet.

Copyright © 2025 Reports in Mechanical Engineering.
All rights reserved.

Corresponding Author:

Mohanad Kadhim Mejbel
Middle Technical University, Technical Engineering College-Baghdad, 10074 Baghdad, Iraq
Email: mohanad@mtu.edu.iq

1. Introduction

The study relates to a new method inspired by the traditional method of the FSSW process (Chen et al., 2017; Dong et al., 2016; Ojo et al., 2015; Reimann et al., 2017; Uematsu et al., 2008; Yu et al., 2022), which can be applied in the automotive industry, as this industry tends to use light metals such as aluminum instead of iron to reduce weight, energy, consumption of fuel, and preserve the environment (Mejbel & Abdullah, 2025). The new method can also be used to manufacture electrical appliances that use spot welding in their production lines due to its high durability, and because the new method improves the appearance of the spot welding, as the shoulder effect has disappeared from the surface of the welded plate (Abdullah et al., 2020a; Mohammad et al., 2022). This effect is considered one of the determinants of using spot welding using the traditional friction stir method in the industry because it is viewed as a deformation (Chen et al., 2017; Paidar et al., 2022; Rosendo et al., 2011). In the conventional method, the mixing tool consists of the mixing rod and the shoulder that rotates at a known rotational speed and penetrates the upper plate to reach the lower plate. It penetrates to a certain depth (Abdullah & Hussein, 2018; Abdullah et al., 2025). At the same time, the shoulder has been embedded in the upper plate for a known distance, after which the mixing tool is lifted to move to another place. Thus, FSSW is obtained. This technique can be repeated to gain many welded points for the same joint (Abdullah et al., 2024; Abdullah & Hussein, 2019). One of the known disadvantages of the traditional

method is the defect left by the rod and shoulder on the surface of the welded plates, which limits its use in industry, especially in visible arjointreduces the joint efficiency. One of the most significant drawbacks is the residual keyhole that remains after the welding process is completed (Fan et al., 2023; Rao et al., 2017). It also limits its use for welding thin plates due to the high heat that results from the frictional force between the shoulder and the upper surface, which leads to the perforation of the upper plate (Ikumapayi & Akinlabi, 2019; Zhang & Gang, 2014). The new method is considered a solid-state welding process (Bergmann et al., 2013) because the welded sheets do not melt, unlike the case when using an electric resistance spot welding process. Therefore, the problems associated with melting, such as bubbles, protrusions, or changes in the microscopic structure of the metals, will disappear, in addition to the issues resulting from corrosion of the welding electrodes, especially when welding aluminum sheets due to the high conductivity of this metal (Chen et al., 2024). We must not forget to mention here the vapours and gases (Popović et al., 2014) associated with the use of the electric resistance welding method, which are considered environmental pollutants (Oudah et al., 2021), and more than this, the high energy required for spot welding using the electric resistance method when compared to this new method. Most prior research on the FSSW of aluminum alloys has focused on the lap arrangement (Abdullah et al., 2021). Research on FSSW of aluminum alloy in a butt configuration has been little documented up to now, as far as we are aware, as a face filler is placed on the sheets to be welded. At the same time, the filler is under the rotating tool. We could weld the metal sheets together in a butt-joining configuration using a face filler and obtain a very acceptable result. It led to reducing the weight of the welding joints, which in turn lowered production costs. Also, using the filler with small dimensions provides high efficiency in joining. Therefore, this study investigates the FSSW of aluminum alloy in a butt configuration in response to a particular need from the automotive component manufacturing industry. It also became possible to weld thin sheets with a thickness of less than 1 mm in a butt manner without the presence of the known defects that appear in the traditional FSSW welding method. The basic idea in this method is the process of welding two aluminum sheets in a butt configuration and obtaining a butt-welding joint without any defects, i.e., without a keyhole, voids, holes, or cracking.

2. Experimental Work

2.1 Materials

The FSSW joints were welded from aluminum alloy AA 1050 (Kaiser Aluminum, USA) in a butt configuration having a dimension of (2 x 25 x 100 mm). The weldments were made according to the American Welding Society (AWS C1.1M/C1.1:2012), as shown in Figure 1. According to the manufacturer's MSDS datasheet, the aluminum alloy chemical composition is (99.6% Al, 0.04% Cu, 0.1% Fe, 0.029% Mg, 0.049% Mn, 0.12% Si, 0.01% Ti, 0.022% V, 0.03% Zn). Its mechanical characteristics are listed in Table 1. The FSSW joints were carried out using a pin-less cylindrical tool made from high-speed steel grade ASTM M2 (length = 100 mm and diameter = 16 mm), as illustrated in Fig. 1, to avoid the generation of a probe keyhole that lowers the joint mechanical characteristics (Akinlabi et al., 2017).

Table 1: AA1050 Mechanical Characteristics

AA 1050	Shear Strength (MPa)	Yield Stress (MPa)	Tensile Strength (MPa)
2 mm Sheet	69	105	110

2.2 Mechanical and Microstructural Characterisation

To study the microstructure of this alloy, a specimen was obtained from the welded zone of the AA1050 sheets and examined with an Olympus optical microscope (OM, Japan) equipped with a digital camera, with a magnification range of 20 to 400X, per ASTM-E407. The specimen surface was sanded and polished using several grades of emery sheets to expose the overall structure of the AA1050 alloy (200 to 4000 microns). To achieve a mirror quality, the specimens were cloth-polished with an addition of 0.25 µm alumina paste. Keller's etcher, a chemical etching solution for polished samples, consists of 2.5 ml HNO3, 1.4 ml HCl, 100 ml distilled water, and 0.95 ml HF. By swabbing with cotton that has been soaked in the etched for around twenty seconds, the majority of etchants can perform their functions most effectively (Abdullah et al., 2020a, 2020b; Hussein et al., 2019). Microstructural investigations were performed at higher magnifications using a scanning electron microscope (model TESCAN-VEGA/USA) per ISO 22493:2014 to investigate the morphology of the cracked edges after tensile testing with a voltage operation of 50 kV (Ali et al., 2022; Beddai et al., 2022). The local resistance to plasticity along three measurement lines at different levels was evaluated using a microhardness tester to better study the local changes in the mechanical characteristics of different bonded areas. To quantify Vickers hardness in compliance with ASTM E384, a Laryea digital micro-

hardness instrument was used. Each indentation was spaced 250 µm apart, the dwell period was 10 seconds, and a static loading of 100 grams was used as the test setting. Three levels on a horizontal line were measured; the first level was executed below 0.5 mm from the upper cross-sectional surface of the bonded sheets. The second level was 1 mm, and the third was 1.5 mm. According to the ASTM-E8 standard, tensile tests were conducted on the specimens at a quasi-static speed of 1.5 mm/min to assess their tensile bonding strength. To test the welded sample, the machine jaw was clamped down on it. The response force was documented on the displacement force curve during tensile deformation. A universal tensile testing machine (Laryee 50 kN, China) was used to conduct the tests. We ran each setup parameter three times for more reliable results.

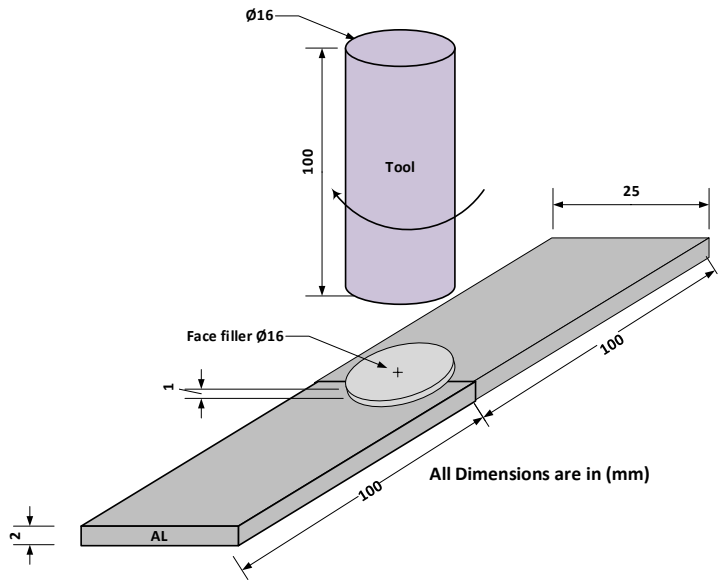

Figure 1: Welding Joint Configuration

2.3 Face Filler

The face filler is a disc made from the same metal as the AA1050 sheets. Its thickness is equal to half the thickness of the plate (1 mm). Its diameter equals the tool diameter (16 mm). The face filler is placed on the ends of the plates required to be welded in a butt configuration and in the centre where the ends of the sheets meet. The face filler is vital because it is the main factor in connecting the required sheets. Therefore, when the rotating tool presses on the surface of the face filler during the welding process and advances vertically downward a distance equal to the thickness of the face filler, it completes the welding without leaving a trace on the surface of the welded sheets, as happens in the traditional FSSW and eliminates the defect (keyhole) that FSSW suffers from. The face filler is manufactured using a special mould to prepare it. The mould consists of two main parts: the first part is the punch, 16 mm in diameter, and the second part is the die, with a diameter of 16.1 mm. See Fig. 2.

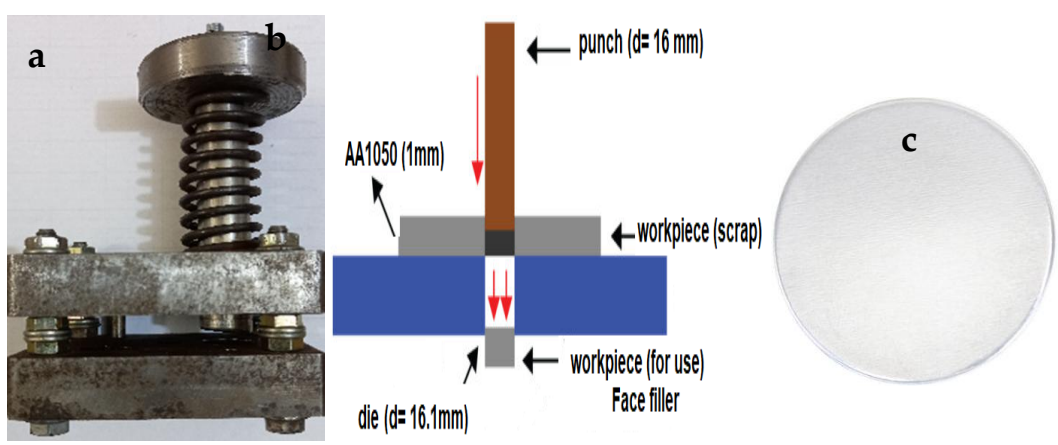

Figure 2: (a) Special Mould to Produce the Face Filler. (b) Schematic Drawing of the Mould. (c) Face Filler.

2.4 Welding Machine

A classic milling machine of the type TOZ was used in this work to carry out the welding process (Mejbel et al., 2021), where the machine axis rotates at different speeds ranging between 45-1800 rpm (Mejbel et al., 2022) and a feed speed ranging between 16-800 mm/min. In this work, three rotational speeds (1800, 1400, 1120) rpm were chosen, which helped carry out the FSSW. Also, different feed speeds were selected for the tool to descend, which are (16, 25, 40) mm/min perpendicular to the welding area and help in applying the required pressure to carry out the welding process and increase the temperature of the metal, stirring and pressure on the metal sheets to be welded. Finally, after pulling the tool, the welding process takes place between the aluminum sheets.

2.5 Welding Process

The two sheets are placed cross-sectionally using a special arrangement to conduct the welding process. After that, the face filler disc (1 mm thickness and 16 mm diameter) is placed on the two sheets from the same metal required to be welded, which was previously manufactured using a mould, and in the centre of the connection of the ends of the two pieces. Then, the rotating tool (welding tool) plunges downwards against the filler, generating heat. The tool is left rotating without advancing downwards for (2 or 3 seconds) for preheating purposes in some runs, and the tool advances at a known vertical feed (as mentioned in Table 2) on the surface of the filler and the sheets required to be welded for runs without preheat. The filler's temperature rises due to the friction and pressure resulting from the vertical movement of the rotating tool (feed rate), which leads to a flexible deformation in the filler. During this process, heat is transferred from the filler to the two lower sheets to be welded using the spot-welding technique. The distance advanced by the vertically rotating tool equals the thickness of the face filler disk, which is 1 mm. The tool stops advancing downward vertical movement when it reaches the upper surface of the two sheets. This method has been successfully used for welding identical 2 mm thickness of AA 1050 aluminum sheets together in a butt configuration. 27 runs have been executed to perform the welding at different parameters.

Table 2: Welding Parameters

No.	Rotating Speed (rpm)	Preheat Time (sec.)	Depth (mm)	Feed Rate (mm/min)
1	1800	Without Preheat	1	16
2			1	25
3			1	40
4		2	1	16
5			1	25
6			1	40
7		3	1	16
8			1	25
9			1	40
10	1400	Without Preheat	1	16
11			1	25
12			1	40
13		2	1	16
14			1	25
15			1	40
16		3	1	16
17			1	25
18			1	40
19	1120	Without Preheat	1	16
20			1	25
21			1	40
22		2	1	16
23			1	25
24			1	40
25		3	1	16
26			1	25
27			1	40

2.6 Welding Fixture

Figure 3 represents the welding arrangement used to accomplish the new method of spot welding, where this

arrangement consists of the following: 1) The holder: It is a graduated disc with a hole in the middle (the diameter of the hole equals the tool diameter, in addition to the clearance that allows the rotating tool to move inside the hole without obstacles). The benefit of this part is to hold the entire assembly and then hold the sheets placed in a butt shape, i.e., opposite ends, which are required to be welded so that they do not move during the welding process. 2) The support: It is a fixed solid metal piece placed under the sheets to be welded to support the circular filler and the two sheets during welding. 3) The holding disk that holds the circular filler disk and compresses the sheets on the support piece.

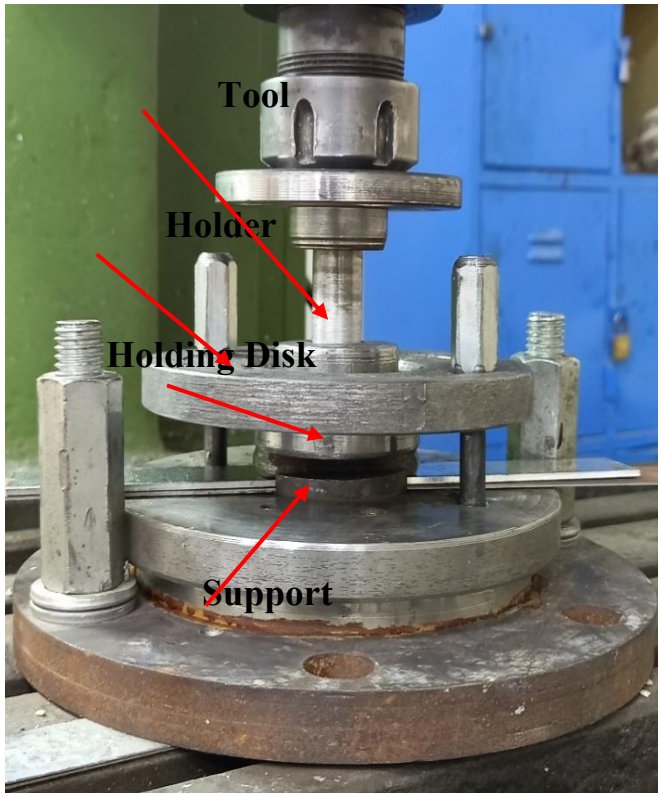

Figure 3: Fixture Assembly

Figure 4 represents the sheets after welding, as fig. 4a shows the two sheets having a stirring impression and a thin flash on their peripheral edge. This thin flash is caused by the softened metal of the filler that was extruded backwards in the clearance between the tool and the holding disk hole. Fig. 4b shows the sheets after removing this metal flash with sandpaper.

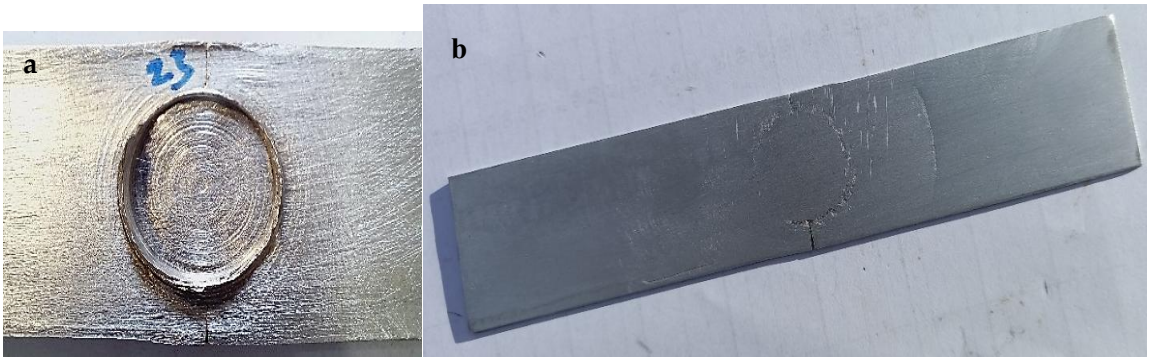

Figure 4: Welded Sheets a) Before Removing the Flash. b) After Removing the Flash.

2.7 Fixture Assembly Steps

Fig. 5 illustrates the exact details of fixing the sheets to be welded. Fig. 5a represents the mould fixed on the milling

machine with the supporting die and the two sheets placed in a butt configuration with opposite faces. Fig. 5b. Place the circular face filler on the sheets in the centre of the facing area. Fig. 5c the holding disk is placed on the sheets, ensuring the filler is in its centre position. Fig. 5d the holder holds the entire assembly tight to ensure no movement occurs during welding. Fig. 5e represents the fixing assembly ready to carry out the welding process after the welding tool touches the face filler, after which the machine is operated. The rotation process occurs, and the welding tool descends by a distance of 1 mm to carry out the welding process.

Figure 5: Fixture Assembly Steps From (a) to (e).

3. Results and Discussion

3.1 Tensile Testing

To evaluate the weld strength of the butt joints, the welded samples were examined by measuring the tensile force required to cause failure using a Chinese-made tensile machine with a capacity of 50 KN (5 tons) and a test speed of 1.5 mm/minute. It was considered to examine three samples under the same conditions and then calculate the average tensile force and strength required to cause failure. Fig. 6 illustrates the average results of max. The tensile loads required to separate the welded plates failed. Fig. 7 illustrates the average results of max. failure tensile strength. The best result of the applied force to break the weld was 4000 Newton at run no. 20, with a bonding efficiency ratio of 72% from the original metal failure load. The tensile strength to break the weld was 125 MPa, with a bonding efficiency ratio of 113.6% of the original metal strength. Run no. 20, which represents the best welding condition, showed the presence of plastic behavior at the weld zone after reaching the maximum load in addition to the appearance of high ductility of more than 7 mm during the tensile test, which is an indication of good weld quality, see Fig. 8. The tensile test for this sample also witnessed a continuous curve without any interruptions or sudden drops in strength, which is another indication of good weld quality and the absence of defects in the weld.

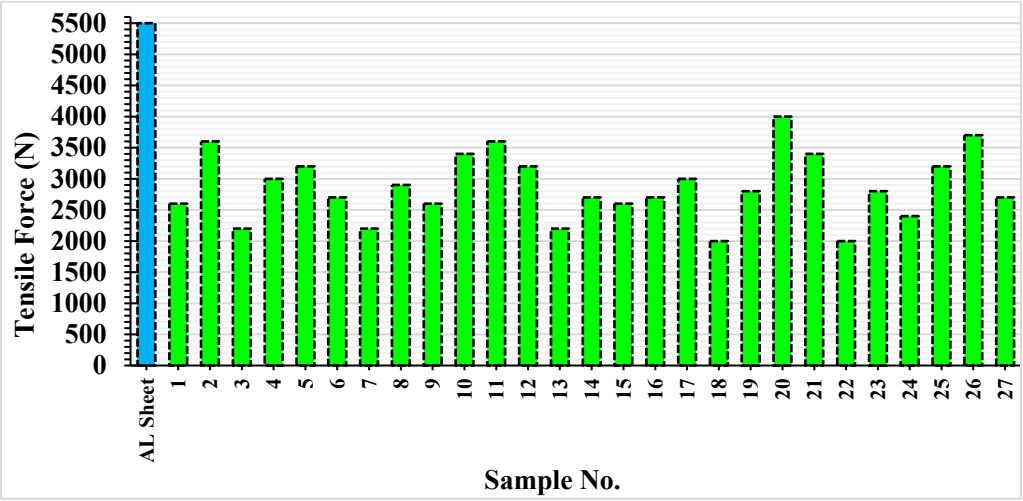

Figure 6: Average Tensile Failure Force for all 27 Runs.

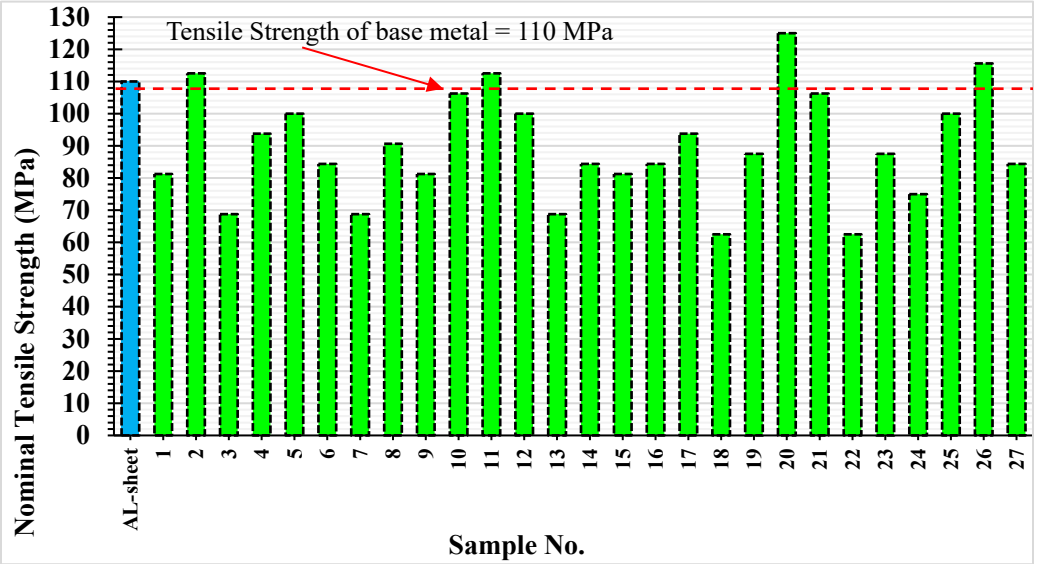

Figure 7: Average Tensile Strength for all 27 Runs.

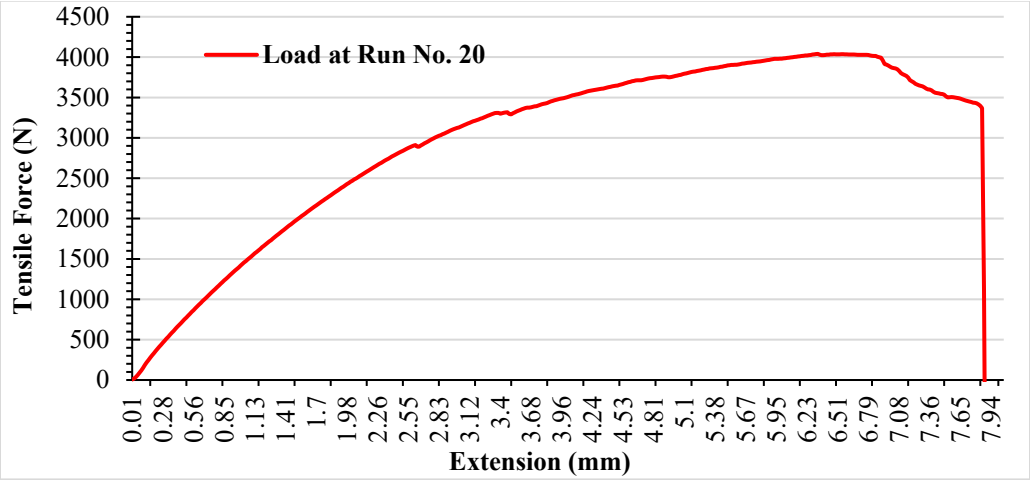

Figure 8: Tensile Force Curve of Run no. 20.

3.2 Micro Hardness

Figure 9 shows the microhardness measurement on the joint cross-section bonded at run no. 20. Three lines of measurement were taken 0.5, 1, and 1.5 mm below the upper sheet of the welding joint, and the spacing distance between each indentation was 250 µm. It is generally known that heat exposure during FSSW controls weld zone hardness via thickness (Xu et al., 2021). After FSSW, the beginning material condition impacts hardness. Excessive heat exposure should reduce weld hardness by coarsening (Heidarzadeh et al., 2021). This investigation shows that the hardness curves over the weld zone transverse cross-section accurately represent hardness behaviour. The Al Base Metal (BM) had mean hardness values of 38 ± 2 HV. The generated heat of friction resulted in a significant reduction in the weld zone hardness of 27.8 HV in comparison to the BM (Tao et al., 2016). The Heat-Affected Zone (HAZ) showed the lowest hardness values in the weld zone because of the grain structure, which is clear after 5 to 7 mm from the centerline on both sides where the hardness measurement started (Aydin et al., 2017; Tunçel et al., 2020). In this area, the hardness values dropped dramatically to reach 27.8 $HV_{(100)}$, representing the HAZ zone. Because of its dynamically recrystallized structure of equiaxed tiny grains that may occur throughout the cooling cycle, the stirring zone (SZ), on the other hand, exhibited a greater hardness of 34 - 36 $HV_{(100)}$, which was recorded at the first few micrometers from the centerline (Kesharwani et al., 2024). At the centre of the SZ, where dynamic recrystallisation and intense plastic deformation occur, lies the Dynamic Recrystallisation Zone (DRZ), where the highest hardness is found. Increased heat energy during the intense stirring process significantly refines the grains, which explains the observed effect. The primary method in plastic deformation is dislocation mobility; smaller and more equiaxed grains may restrict this movement, increasing mechanical strength (Muhayat et al., 2025). Hardness levels for the Thermo-Mechanical Affected Zone (TMAZ) are lower than those for the SZ and more significant than those for the HAZ. One possible explanation for why the TMAZ hardness is higher than the HAZ is that the FSSW technique promotes a large density of dislocations developed by plastic deformation (Baudin et al., 2023; Sato et al., 2001). On the other hand, temperatures in the HAZ are shown to have the lowest hardness ratings. In this particular location, the material does not experience a large amount of plastic deformation, yet it is subjected to substantial temperatures during welding. Consequently, grain coarsening occurs, resulting in a decrease in hardness (Abdullah et al., 2025; Luo et al., 2016). Attention should be drawn to a precise observation, which is the presence of a difference in the locations of the lowest hardness for each line, as it was found that the yellow line had the farthest horizontal distance of the lowest hardness point of ±7 mm from the centerline. In contrast, the lowest hardness point in the red line is closer to the rotating centerline with a distance of ±5 mm, and this is due to the presence of an oval shape distribution of the filler face metal edges inside the aluminum welded sheets, due to plastic deformation caused by the stirring action. The lowest hardness point in the blue line is ±6.5 mm away from the center of rotation.

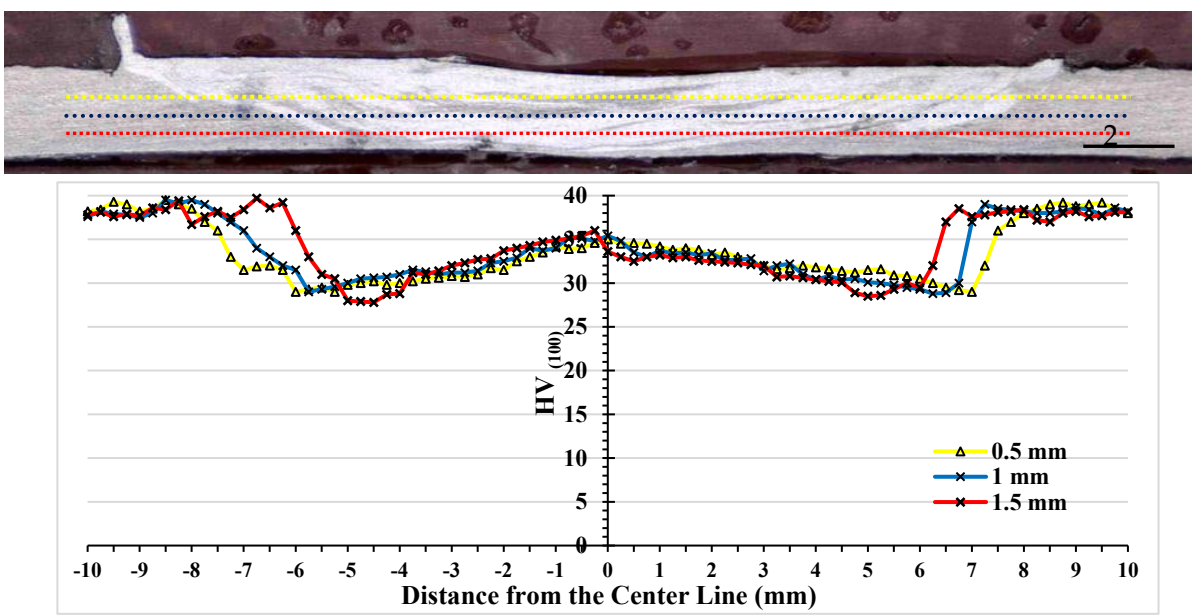

Figure 9: Vickers Microhardness Values and their Locations Across a Horizontal Line Made by three Measuring Levels. The First Measurement Level, As Shown in the Dotted Yellow Line, is Below the Upper Sheet Surface of 0.5 mm; the Second Measurement Level, as Shown in the Blue Dotted Line, is 1 mm; the Third Measurement Level, as Shown in the Red Dotted Line, is 1.5 mm.

3.3 Shape of Specimens Before Tensile Test

Table 3 shows the 27 specimens butt welded before breaking them in the tensile test. Images of the welded samples are taken from the front and the rear sides with no defects. The front side of all specimens revealed a ring flash representing the backward extrusion that occurred during the stirring process, as some of the filler metal flows backwards in the clearance between the tool and the holding disk; this clearance is around 0.5 mm. Black traces in the root side are shown in most of the weldments, indicating that the heat generation during the process reached the lower surface of the sheets. Almost all samples exhibit incomplete welded edges, primarily due to the tool and filler sizes of 16 mm, which prevented the welding operation from reaching the remaining sheet width. These incomplete welded edges are around 4.5 mm per side, which is reasonable since the width of the sheet is 25 mm. The root side of samples 13, 21, and 22 witnessed an edge twisting of the contacting sheet ends, and this might be attributed to the high heat generated in the lower layer of the sheet and good mixing of the filler with the base metal leading to a stirring action of the soft metal in that area that reached the lower sheet surface causing the ends of the sheet to twist to the same direction of the rotating tool.

Table 3(a): Specimens before Breaking in the Tensile Test

No.	1	2	3	4	5
Face			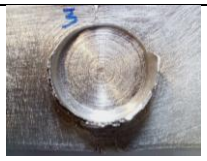		
Bottom	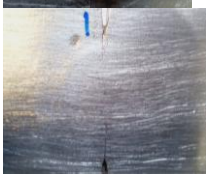	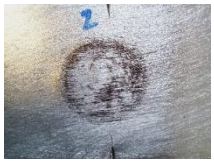	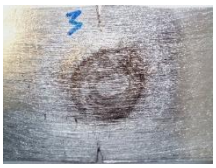	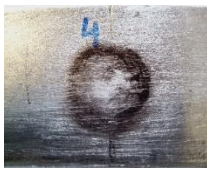	
No.	6	7	8	9	10
Face		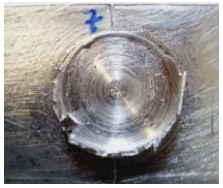	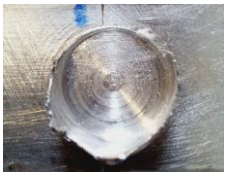		
Bottom		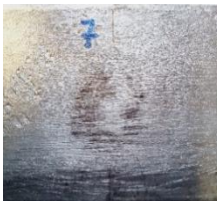		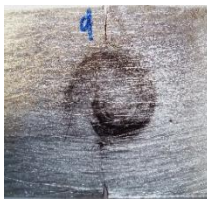	
No.	11	12	13	14	15
Face					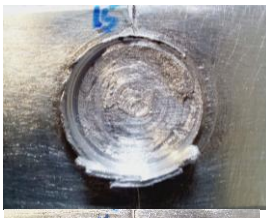
Bottom					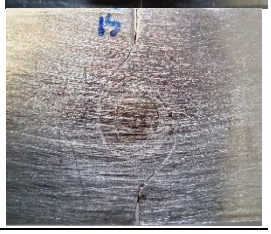

Table 3(b): Specimens before Breaking in the Tensile Test

No.	16	17	18	19	20
Face					
Bottom			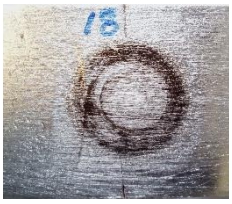	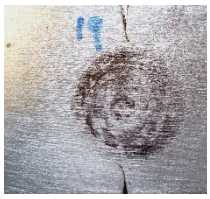	
No.	21	22	23	24	25
Face	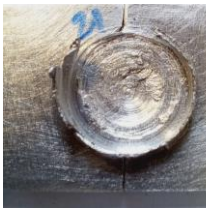		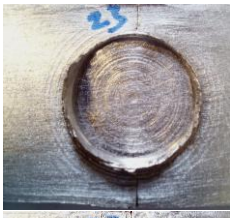		
Bottom				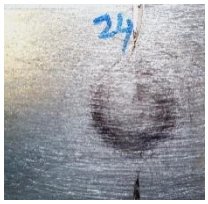	
No.	26	27			
Face					
Bottom					

3.4 Shape of Specimens after Tensile Test

Table 4 shows the 27 specimens butt welded after breaking them in the tensile test. Images of the welded samples are taken from the front and the rear sides. The specimens that were analysed showed two different ways of failure. The welding specimen characteristics and the applied tensile load determine the types of failure:

3.4.1 A Mechanism for the Base Metal Sheet to Fail Via Spot Circumferential Shear

At least a few of the examined aluminium specimens failed in this manner. It happened on the side sheet in the spot's perimeter. See the shape of specimens following the tensile test for evidence that the top sheet may have been severely plastically deformed due to adhering to the revolving tool, which might explain this failure mechanism. (16 to 25).

3.4.2 Mixed Failure Mode.

A tensile failure mode at the interface between the lower sheets and the face filler, and a shear failure in the top sheet occurred at a place smaller than the tool's diameter, see Figures 21, 22. The face filler's plastic deformation and swirling movement formed a mechanical link with the bottom sheets, which led to this failure mechanism, as seen in figures 6, 8, 9, and 10.

Table 4(a): Specimens after Breaking in the Tensile Test

No.	1	2	3	4	5
Face					
Bottom	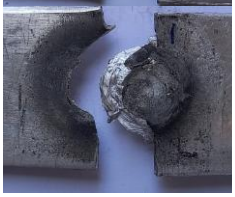	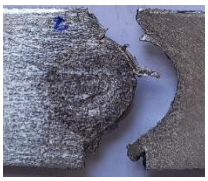			
No.	6	7	8	9	10
Face					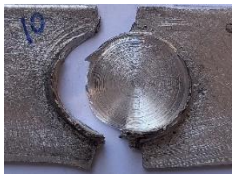
Bottom	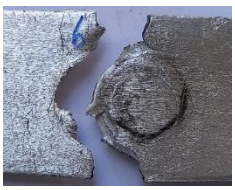			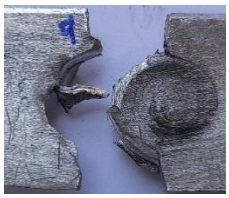	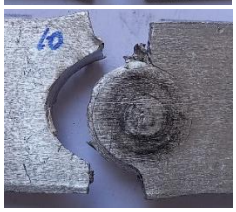
No.	11	12	13	14	15
Face				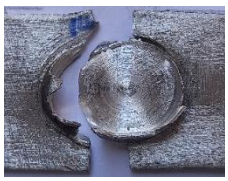	
Bottom				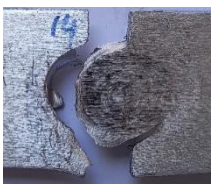	
No.	16	17	18	19	20
Face					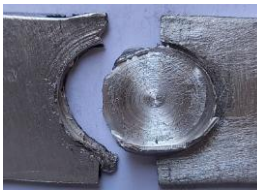

Table 4(b): Specimens after Breaking in the Tensile Test

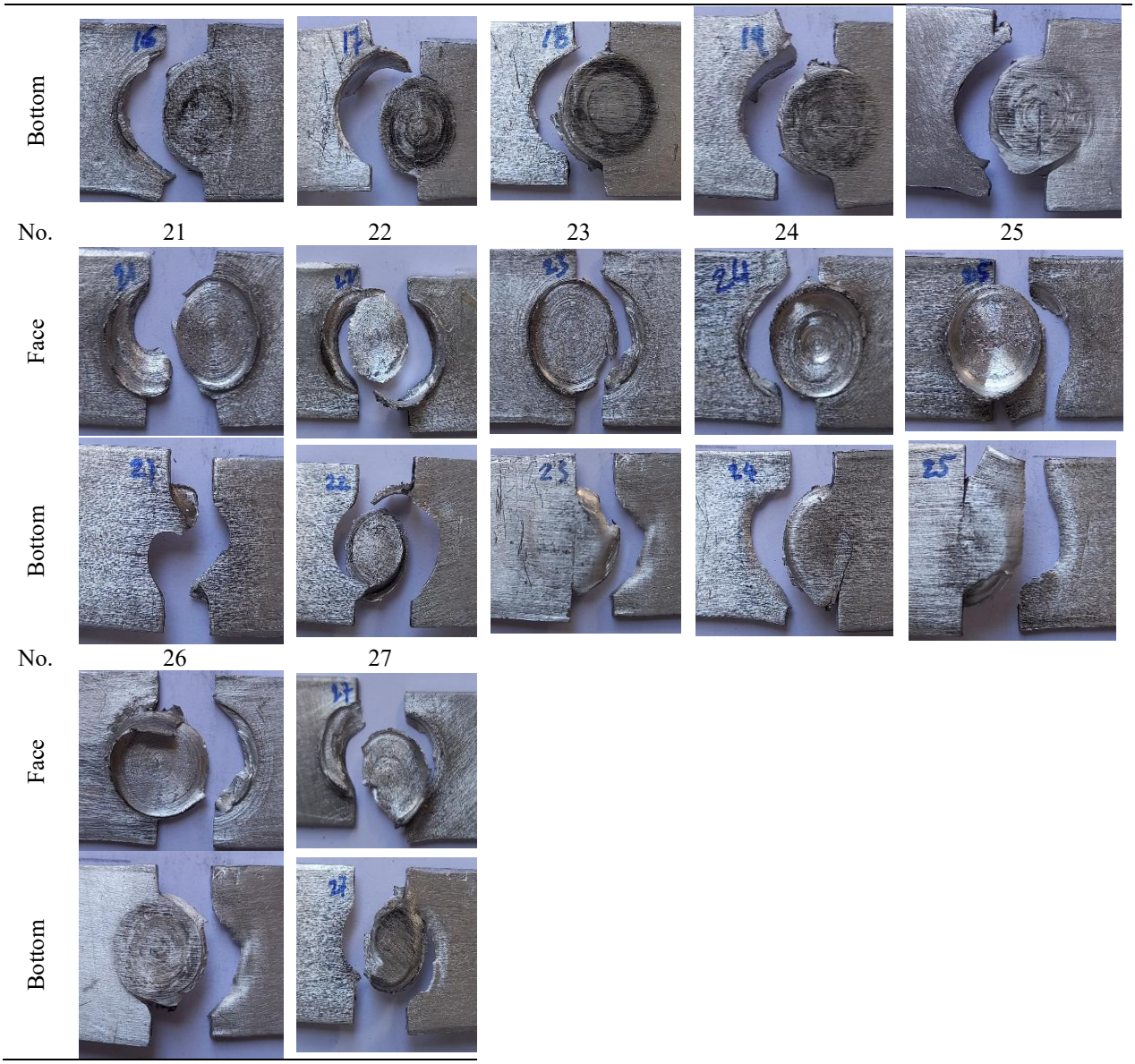

3.5 Microstructure of Sample 20

Figure 10a shows the microscopic appearance of the cross-section for the best-welded specimen mechanical properties made by the face filler friction stir spot welding process (run no. 20). The cross-section illustrated in Fig. 10a reveals distinct zones with various structures. Fig. 10b shows the negative image of Fig. 10a to reveal more details of the stirring zone and how the colors differ from the sheets' base metal. The dark areas in Fig. 10b, located in the middle, represent the filler material after stirring was taken action. The light areas are the detached layers of the lower parts of the sheets' edges, which were colder than the filler material because of its different vertical positions, as the metal near the tool is always higher in temperature compared to the metal far away from the tool; thus, these islands appeared in the stirring zone. These islands are the segments of the sheets' base metal and are detached due to friction and stirring action, and are distributed in the SZ, see fig 10d,e,f,g,h,k. In doing so, a symmetric welding is produced. The FSSW face filler compresses the filler substance downwards as the tool rotates. As a result, the material under the tool may be vigorously stirred. During this period, the face filler is forged and twisted in the base metal (BM) of both sheet edges, and metallurgical bonding between the filler and BM occurs. Considering that there is no distinct delineation between the sheets, this is evident from the photos and the enlarged details, see Fig. 10a,b. Figure 10 (d, h, i, m) exhibits lamellar structure due to non-uniform temperature gradient mixing of face filler and base metal during

welding (Alizadeh-Sh et al., 2024; Huang et al., 2023; Mejbel et al., 2025; Van et al., 2019; Wang et al., 2024). The nugget zone indicates onion rings and thermally stable microstructure, as shown in fig. 10 (c, j, l). Onion rings are made up of banded structures that alternate with one another and have varying grain sizes and phases. Several researchers believe that this layered stacking structure, which has a variety of structures and features, has the potential to contribute to the impact of layered strengthening, which increases both strength and plasticity concurrently. Microcracks were revealed at the middle thickness of the sheets, as shown in Fig. 10 (m, n), particularly near the HAZ zone as the result of residual stresses from the base material restraining the weld. This leads to structural changes in the metal that weaken the part in this area. The mechanical properties are affected.

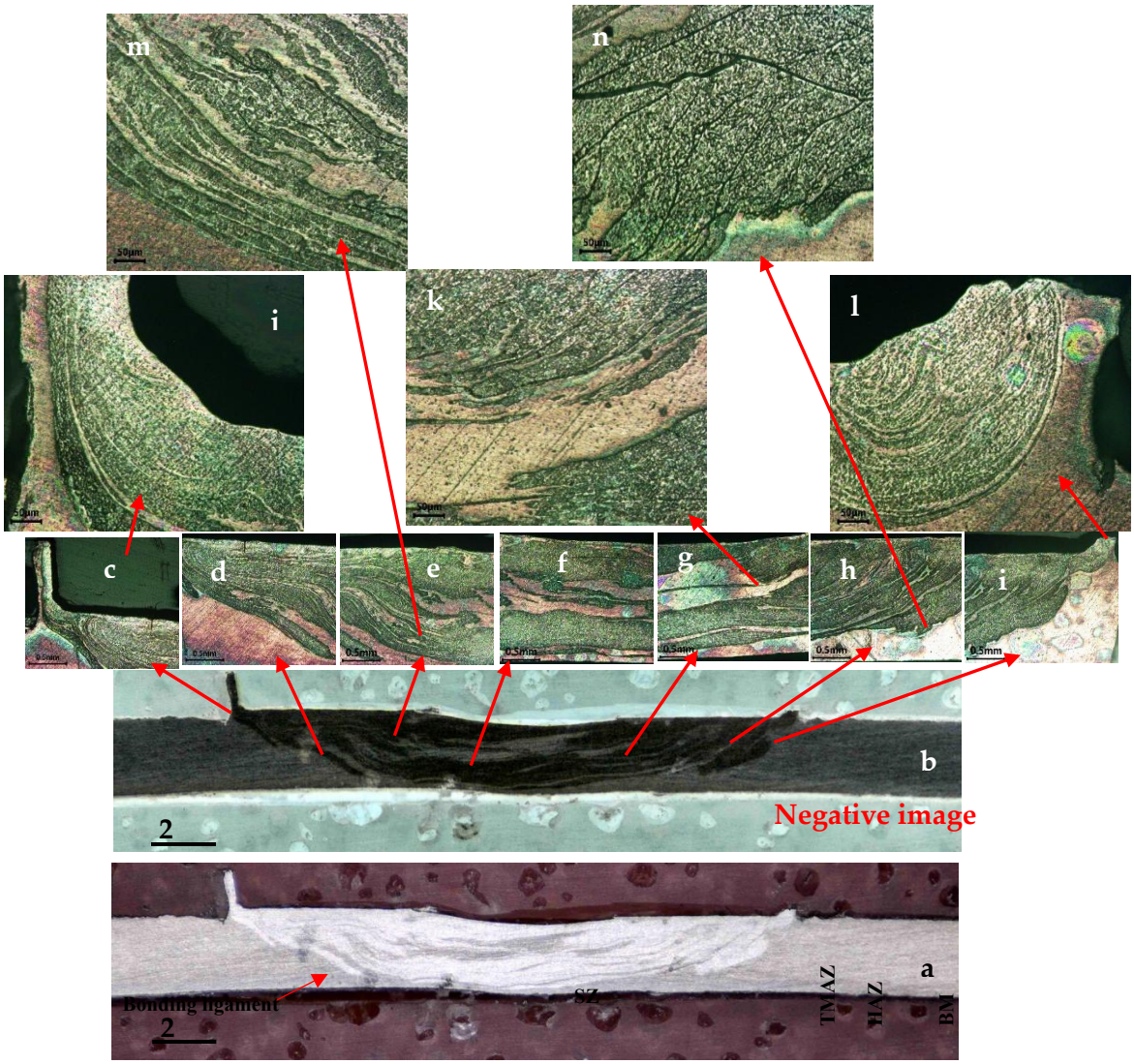

Figure 10: Optical Microstructure of Sample 20.

3.6 SEM and AFM of Sample 20

SEM analysis was undertaken from the inside fracture surfaces of the broken specimen no. 20 at the peripheral edge, see Fig. 11. The fracture surface was viewed at multiple magnifications. The metal of the two sheets suffers from severe plastic flow during this welding procedure. This flow results from several variables, such as the frictional heat generation, the increased loading between the rotating tool and the face filler, and the tool's rate of feed. These factors force the filler and plates to move and flow beneath the rotating tool in a vortex-like pattern, bringing the oxide-free surfaces together for the weld. These images show that the metal beneath the rotating tool has suffered softening due to the heat and frictional loading imposed by the revolving tool. This results in the fillet metal and the plates being forced to adhere to the tool and rotate in a vortex. This vortex occurs in the space between the tool and

the lower anvil, on which the plates are positioned, where the revolving tool's tangential reaction force shears it. This image provides an observation of the metal flow during the welding procedure. This flow is necessary to break down the oxide layer and bring the pure metal of both sheets into contact with the fillet to achieve a weld. It is possible to make a precise determination that failure occurs at the boundary between the two sheets, which is located across the nugget zone (NZ), and that the whole surface of the sheets has been sliced. Relatively prominent ridges are visible around the fracture surface. The crack propagation area is highlighted to provide a deeper and more expanded view of the cracking process. The crack begins at the bottom of the nugget zone and moves circularly toward the centre of the weld. It also moves in the direction of the circumference of the structure. Indicating that the fracture is primarily focused in the region around the nugget zone is the occurrence of a significant number of shear dimples during the tensile test, which may be found in various amounts and sizes. Small cracks are also noticeable on the right side of the second image at 61x magnification. The load distribution and structural integrity are both impacted by the morphology of the peripheral interface, which plays a direct role in determining the joint failure load. Stress concentrations may be caused by fractures or cavities inside the interface, which can weaken the joint and reduce its ability to sustain load. On the other hand, a well-bonded smooth interface increases uniform stress distribution, enhancing the joint's capacity to withstand larger loads before it fails (Rishad et al., 2025; Shi et al., 2018) . There are ridges around the periphery of the nugget zone, indicating the possibility of a fracture that may propagate in this direction. In addition, some elongated dimples can be seen in the 150X, 300X, and 600X magnification images, which reveal the sheets' impressive bonding capabilities when magnified.

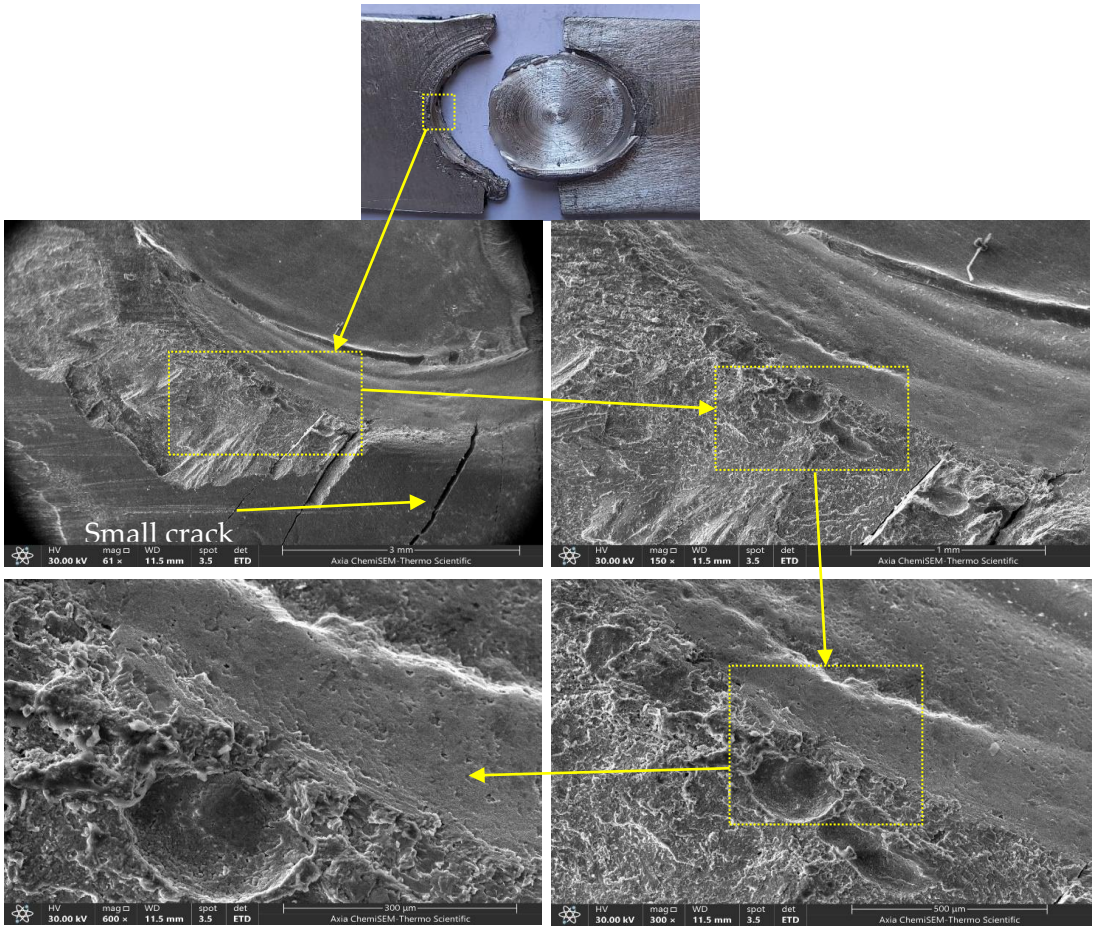

Figure 11: SEM Images of Sample 20.

Multiple studies have examined the association between morphologies and joint failure load, revealing different yet essential findings. Weld stress distribution and magnitude are drastically affected by morphological changes like voids, fractures, or imperfect bonding. The total load-bearing capacity of the joint may be reduced due to increased stress concentrations brought about by these fluctuations. To guarantee an equal load transmission, the surface uniformity and smoothness of the interface are of the utmost importance. This directly influences the joint's capacity

to tolerate larger loads, which in turn increases the joint failure load (Rosendo et al., 2011). Figure 12 shows the 3D surface morphology of the inner surface of the sheets after fracture, as well as the underside of the sheet. An Atomic Force Microscopy (AFM) microscope was used to capture a 3D image with a scanning area of 5 µm x 5 µm. Figure 12a shows rough fracture zones with clearly defined thick dimples in mountains and valleys, approximately 2 µm high or slightly less, indicating a ductile fracture, as this area represents the peripheral edges of HAZ. Figure 12b shows the fracture zone slightly outside the nugget zone, representing the original base metal of the sheets. It is noticed that the fracture surface is less rough than the nugget zone, and there are fewer hills with heights less than 2 µm, with thinner dimples formed (Kubit et al., 2025; Prihajatno et al., 2024).

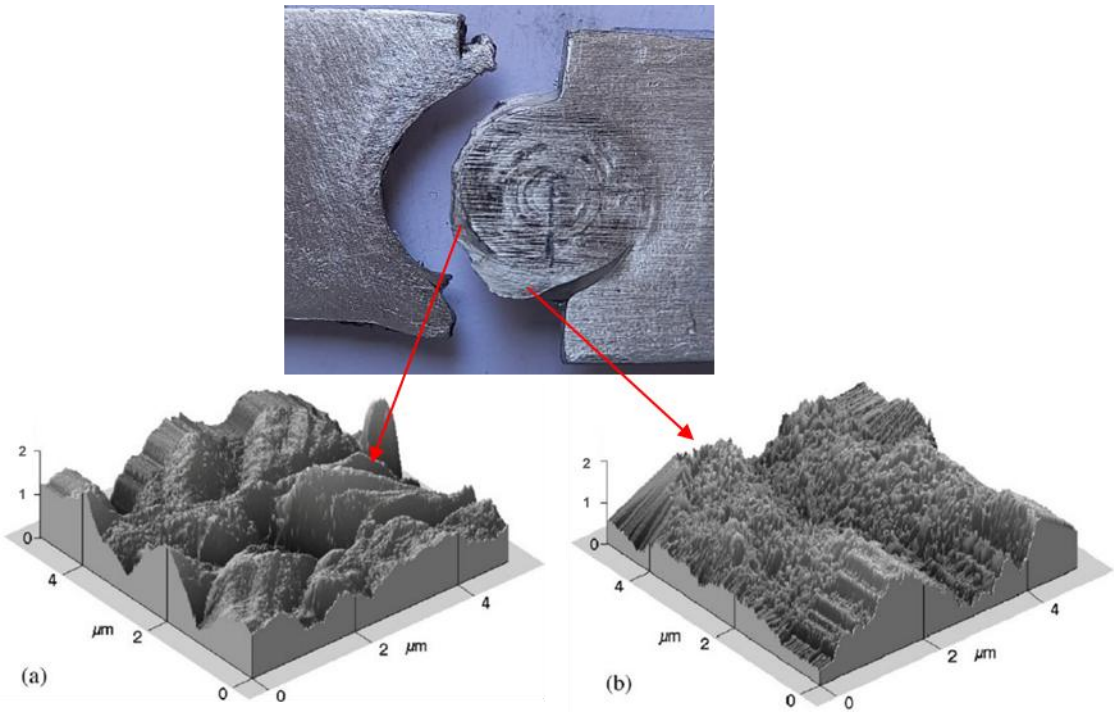

Figure 12: AFM Images of Sample No. 20.

4. Conclusions

In this work, a face filler friction stir spot welding process of similar AA1050 was successfully performed in a butt joint configuration by using a face filler disk from the same alloy of 1 mm thickness. Three rotational speeds (1120, 1400, and 1800 rpm) with a linear movement perpendicular to the facial filling and then to the sheets were used. The samples were welded with and without preheating, with the stirring tool lowered by 1 mm in a vertical orientation. The following conclusions may be drawn:

1- According to the findings, this innovative face filler friction spot welding procedure was found to be effective for spot welding both thin and thick sheets, as well as comparable and dissimilar combinations.

2- With the elimination of the keyhole, considered a flaw in the standard friction stir spot welding procedure, it was possible to obtain keyhole-less areas while maintaining adequate joint strength.

3- This method is cost-efficient compared with other processes.

4- This process can be performed in two ways: butt-shape and lap-shape welding.

5- No matter what, the tool's descending depth cannot exceed the face filler disc's thickness.

6- Welding sheets of varying thicknesses (0.5 or 1.0 mm) and types of aluminium (similar or different) is possible with this procedure.

7- The best welding parameters were (1120 RPM) of tool rotation and welding speed (25mm/min), depending on tensile strength.

8- The metallurgical bonding between the face filler disc and the lower sheet causes the disc to become a part of the spot when inserted into the lower sheet.

This study may open the way for further research into welding with new alloys, both similar and different to those previously researched. This is because the presented procedure is innovative and has tremendous potential for further

inquiry. It is recommended that in future work, a numerical assessment model with measured geometry, adjusted material properties, and residual stress distribution may be able to cover the majority of the mechanical results that are supplied by the processing parameters. This well-established analytical technique is both accurate and helpful when it comes to mechanical modelling.

Authors' Contributions

First Author: testing, experimental work, funding, and idea concept.

Second Author: evaluation, discussion, manuscript writing, and final proof.

Data Availability

The data that support the findings of this study are available from the corresponding author upon reasonable request.

References

Abdullah, I., Mejbel, M., & Al-bhadle, B. (2024). Double stage friction stir spot extrusion welding: a novel manufacturing technique for joining sheets. *Experimental Techniques*, *48*(2), 323-342. https://doi.org/10.1007/s40799-023-00660-2

Abdullah, I., Ridha, M., Barrak, O., Hussein, S., & Hussein, A. (2021). Joining of Aa1050 sheets via two stages of friction spot technique. *Journal of Mechanical Engineering Research and Developments*, *44*(4), 305-317. https://www.researchgate.net/profile/Osamah-Barrak/publication/351069050_Joining_of_Aa1050_Sheets_Via_Two_Stages_of_Friction_Spot_Technique/links/6082c827907dcf667bba2119/Joining-of-Aa1050-Sheets-Via-Two-Stages-of-Friction-Spot-Technique.pdf

Abdullah, I. T., & Hussein, S. K. (2018). Improving the joint strength of the friction stir spot welding of carbon steel and copper using the design of experiments method. *Multidiscipline Modeling in Materials and Structures*, *14*(5), 908-922. https://doi.org/10.1108/MMMS-02-2018-0025

Abdullah, I. T., & Hussein, S. K. (2019). Shear strength and temperature distribution model of friction spot lap joint of high density polyethylene with aluminum alloy 7075. *International Journal of Structural Integrity*, *10*(4), 469-483. https://doi.org/10.1108/IJSI-05-2018-0025

Abdullah, I. T., Hussein, S. K., & Hussein, A. K. (2020a). Joining of AA6061 to polyvinyl chloride via hot extrusion. *International Journal of Structural Integrity*, *11*(2), 286-302. https://doi.org/10.1108/IJSI-08-2019-0081

Abdullah, I. T., Hussein, S. K., & Hussein, A. K. (2020b). Joining aluminium alloy to pre-holed carbon steel using the aluminium extrusion method with friction spot welding. *International Journal of Structural Integrity*, *11*(6), 849-860. https://doi.org/10.1108/IJSI-10-2019-0112

Abdullah, I. T., Mejbel, M. K., & Al-Filfily, A. A. (2025). Joining 1.1-and 2.1-mm Al Sheets by Friction Stir Spot Welding. *Material Design & Processing Communications*, *2025*(1), 3110429. https://doi.org/10.1155/mdp2/3110429

Akinlabi, E. T., Sanusi, K. O., Muzenda, E., & Akinlabi, S. A. (2017). Material behaviour characterization of friction stir spot welding of copper. *Materials Today: Proceedings*, *4*(2), 166-177. https://doi.org/10.1016/j.matpr.2017.01.010

Ali, K. G., Muhmmed, A. A., Taieh, N. K., & Mejbel, M. K. (2022). Tribological and mechanical performance of epoxy reinforced by fish scales powder. *Revue Des Composites et Des Matériaux Avancés*, *32*(3), 149. https://doi.org/10.18280/rcma.320306

Alizadeh-Sh, M., Fæster, S., Farahani, E., Sarhadi, A., Tiedje, N., Eder, M., & Danielsen, H. (2024). Microstructural evolution during welding of high Si solution-strengthened ferritic ductile cast iron using different filler metals. *Metallurgical and Materials Transactions A*, *55*(7), 2309-2323. https://doi.org/10.1007/s11661-024-07399-4.

Aydin, H., Tuncel, O., Umur, Y., Tutar, M., & Bayram, A. (2017). Effect of welding parameters on microstructure and mechanical properties of aluminum alloy AA6082-T6 friction stir spot welds. *Indian J. Eng. Mater. Sci*, *24*(3), 215-227. https://avesis.uludag.edu.tr/yayin/4ea382f2-2dd3-4008-81c2-ef4f09b56d33/effect-of-welding-parameters-on-microstructure-and-mechanical-properties-of-aluminum-alloy-aa6082-t6-friction-stir-spot-welds

Baudin, T., Bozzi, S., Brisset, F., & Azzeddine, H. (2023). Local microstructure and texture development during

friction stir spot of 5182 aluminum alloy. *Crystals*, *13*(3), 540. https://doi.org/10.3390/cryst13030540

Beddai, A. A., Badday, B. A., Al-Yaqoobi, A. M., Mejbel, M. K., Al Hachim, Z. S., & Mohammed, M. K. (2022). Color removal of textile wastewater using electrochemical batch recirculation tubular upflow cell. *International Journal of Chemical Engineering*, *2022*(1), 4713399. https://doi.org/10.1155/2022/4713399

Bergmann, J. P., Petzoldt, F., Schürer, R., & Schneider, S. (2013). Solid-state welding of aluminum to copper—case studies. *Welding in the World*, *57*(4), 541-550. https://doi.org/10.1007/s40194-013-0049-z

Chen, B.-Q., Liu, K., & Xu, S. (2024). Recent advances in aluminum welding for marine structures. *Journal of Marine Science and Engineering*, *12*(9), 1539. https://doi.org/10.3390/jmse12091539

Chen, K., Liu, X., & Ni, J. (2017). Keyhole refilled friction stir spot welding of aluminum alloy to advanced high strength steel. *Journal of Materials Processing Technology*, *249*, 452-462. https://doi.org/10.1016/j.jmatprotec.2017.06.039

Dong, H., Chen, S., Song, Y., Guo, X., Zhang, X., & Sun, Z. (2016). Refilled friction stir spot welding of aluminum alloy to galvanized steel sheets. *Materials & Design*, *94*, 457-466. https://doi.org/10.1016/j.matdes.2016.01.066

Fan, W., Chu, Q., Yang, X., Li, W., Zou, Y., & Hao, S. (2023). Microstructure and mechanical properties of probeless friction stir spot welded AlLi alloy joints via fast electric pulse treatment: A comparative study. *Materials Characterization*, *205*, 113276. https://doi.org/10.1016/j.matchar.2023.113276

Heidarzadeh, A., Mironov, S., Kaibyshev, R., Çam, G., Simar, A., Gerlich, A., Khodabakhshi, F., Mostafaei, A., Field, D. P., & Robson, J. D. (2021). Friction stir welding/processing of metals and alloys: A comprehensive review on microstructural evolution. *Progress in Materials Science*, *117*, 100752. https://doi.org/10.1016/j.pmatsci.2020.100752

Huang, S., Wang, Y., Fan, M., Huo, X., Ma, N., & Lu, F. (2023). The heterogeneous microstructure of laser welded joint and its effect on mechanical properties for dissimilar 9Cr steel and alloy 617. *Journal of Materials Research and Technology*, *26*, 1094-1106. https://doi.org/10.1016/j.jmrt.2023.07.281

Hussein, S. K., Abdullah, I. T., & Hussein, A. K. (2019). Spot lap joining of AA5052 to AISI 1006 by aluminium extrusion via friction forming technique. *Multidiscipline Modeling in Materials and Structures*, *15*(6), 1337-1351. https://doi.org/10.1108/MMMS-04-2019-0082

Ikumapayi, O. M., & Akinlabi, E. T. (2019). Recent advances in keyhole defects repairs via refilling friction stir spot welding. *Materials Today: Proceedings*, *18*, 2201-2208. https://doi.org/10.1016/j.matpr.2019.06.663

Kesharwani, R., Jha, K. K., Imam, M., Sarkar, C., & Barsoum, I. (2024). Correlation of microstructure, texture, and mechanical properties of friction stir welded Joints of AA7075-T6 plates using a flat tool pin profile. *Heliyon*, *10*(3). https://doi.org/10.1016/j.heliyon.2024.e25449

Kubit, A., Derazkola, H. A., Jurczak, W., Ochałek, K., Myśliwiec, P., Macek, W., Łastowska, O., Podulka, P., & Slota, J. (2025). Effects of process parameters on dynamic and static load capacity of EN AW-2024-T3 aluminum alloy joints prepared by friction stir welding. *Archives of Civil and Mechanical Engineering*, *25*(3), 153. https://doi.org/10.1007/s43452-025-01204-8

Luo, C., Li, X., Song, D., Zhou, N., Li, Y., & Qi, W. (2016). Microstructure evolution and mechanical properties of friction stir welded dissimilar joints of Mg–Zn–Gd and Mg–Al–Zn alloys. *Materials Science and Engineering: A*, *664*, 103-113. https://doi.org/10.1016/j.msea.2016.03.117

Mejbel, A., Khalaf, M. M., & Kwad, A. M. (2021). Improving the machined surface of AISI H11 tool steel in milling process. *J. Mech. Eng. Res. Dev*, *44*(4), 58-68. https://www.researchgate.net/profile/Mohanad-Mejbel/publication/351117059_Improving_the_Machined_Surface_of_AISI_H11_Tool_Steel_in_Milling_Process/links/608856ff907dcf667bcabfec/Improving-the-Machined-Surface-of-AISI-H11-Tool-Steel-in-Milling-Process.pdf

Mejbel, M. K., & Abdullah, I. T. (2025). Friction Stir Spot Extrusion Joining With Its Metal Flow Investigation. *Advances in Materials Science and Engineering*, *2025*(1), 1617392. https://doi.org/10.1155/amse/1617392

Mejbel, M. K., Abdullah, I. T., & Taieh, N. K. (2022). Thin wall manufacturing improvement using novel simultaneous double-sided cutter milling technique. *International Journal of Automotive and Mechanical Engineering*, *19*(1), 9519-9529. https://doi.org/10.15282/ijame.19.1.2022.15.0734

Mejbel, M. K., Hussein, S. K., & Abdullah, I. T. (2025). Friction stir consolidation for recycling AA6061 chips with

its metal flow investigation for billet production. *Journal of Engineering Research*, *13*(2), 1170-1183. https://doi.org/10.1016/j.jer.2024.04.010

Mohammad, S., Daway, E., & Mejbel, M. (2022). Friction Stir Spot Joining of Aa6061-T6 To Fiber Glass Composite Material. *Int J Tech Phys Probl Eng*, *14*(4), 203-210. https://www.researchgate.net/profile/Mohanad-Mejbel/publication/366682745_FRICTION_STIR_SPOT_JOINING_OF_AA6061-T6_TO_FIBER_GLASS_COMPOSITE_MATERIAL/links/63ae35b5a03100368a3b3cdc/FRICTION-STIR-SPOT-JOINING-OF-AA6061-T6-TO-FIBER-GLASS-COMPOSITE-MATERIAL.pdf

Muhayat, N., Larasati, R. D., Putri, E. D., & Budiana, E. P. (2025). Effect of tool diameter on the joint properties of AA6061 hollow panels using a novel one-step double-acting Friction Stir Weld method. *Journal of Advanced Joining Processes*, *11*, 100277. https://doi.org/10.1016/j.jajp.2024.100277

Ojo, O. O., Taban, E., & Kaluc, E. (2015). Friction stir spot welding of aluminum alloys: a recent review. *Materials Testing*, *57*(7-8), 609-627. https://doi.org/10.3139/120.110752

Oudah, M. H., Mejbel, M. K., & Allawi, M. K. (2021). R134a flow boiling heat transfer (FBHT) characteristics in a refrigeration system. *J. Mech. Eng. Res. Dev*, *44*(4), 69-83. https://www.researchgate.net/profile/Mohanad-Mejbel/publication/350107942_R134a_Flow_Boiling_Heat_Transfer_FBHT_Characteristics_in_a_Refrigeration_System/links/6051d29da6fdccbfeae674ae/R134a-Flow-Boiling-Heat-Transfer-FBHT-Characteristics-in-a-Refrigeration-System.pdf

Paidar, M., Bokov, D., Mehrez, S., Nasution, M. K., Ojo, O. O., & Zain, A. M. (2022). The influence of the backing plate materials on microstructure and mechanical properties of friction spot extrusion brazing of AA2024-T3 aluminum alloy and Brass sheets. *Journal of Manufacturing Processes*, *74*, 28-39. https://doi.org/10.1016/j.jmapro.2021.12.002

Popović, O., Prokić-Cvetković, R., Burzić, M., Lukić, U., & Beljić, B. (2014). Fume and gas emission during arc welding: Hazards and recommendation. *Renewable and sustainable energy reviews*, *37*, 509-516. https://doi.org/10.1016/j.rser.2014.05.076

Prihajatno, M., Ilman, M., Sriwijaya, R., Muslih, M., & Apriansyah, R. (2024). Tensile and fatigue properties of friction stir AZ31B-H24 magnesium alloy welded joints under the influences of pin geometry and tool rotation rate. *Journal of Advanced Joining Processes*, *9*, 100202. https://doi.org/10.1016/j.jajp.2024.100202

Rao, H., Jordon, J., Boorgu, S., Kang, H., Yuan, W., & Su, X. (2017). Influence of the key-hole on fatigue life in friction stir linear welded aluminum to magnesium. *International Journal of Fatigue*, *105*, 16-26. https://doi.org/10.1016/j.ijfatigue.2017.08.012

Reimann, M., Goebel, J., & dos Santos, J. F. (2017). Microstructure and mechanical properties of keyhole repair welds in AA 7075-T651 using refill friction stir spot welding. *Materials & Design*, *132*, 283-294. https://doi.org/10.1016/j.matdes.2017.07.013

Rishad, S. M. A., Islam, M. A., & Islam, M. S. (2025). Analysis of stress distribution of CFRP bonded joints: A study of numerical and machine learning approach. *Heliyon*, *11*(3). https://doi.org/10.1016/j.heliyon.2025.e42440

Rosendo, T., Parra, B., Tier, M., Da Silva, A., Dos Santos, J., Strohaecker, T., & Alcântara, N. (2011). Mechanical and microstructural investigation of friction spot welded AA6181-T4 aluminium alloy. *Materials & Design*, *32*(3), 1094-1100. https://doi.org/10.1016/j.matdes.2010.11.017

Sato, Y. S., Park, S. H. C., & Kokawa, H. (2001). Microstructural factors governing hardness in friction-stir welds of solid-solution-hardened Al alloys. *Metallurgical and Materials Transactions A*, *32*(12), 3033-3042. https://doi.org/10.1007/s11661-001-0178-7

Shi, Y., Yue, Y., Zhang, L., Ji, S., & Wang, Y. (2018). Refill friction stir spot welding of 2198-T8 aluminum alloy. *Transactions of the Indian Institute of Metals*, *71*(1), 139-145. https://doi.org/10.1007/s12666-017-1146-2

Tao, W., Yong, Z., Xuemei, L., & Matsuda, K. (2016). Special grain boundaries in the nugget zone of friction stir welded AA6061-T6 under various welding parameters. *Materials Science and Engineering: A*, *671*, 7-16. https://doi.org/10.1016/j.msea.2016.06.050

Tunçel, O., Tutar, M., & Bayram, A. (2020). Effect of tool pin profile on the hook geometry and mechanical properties of a friction stir spot welded AA6082-T6 aluminum alloy. *Transactions of the Canadian Society for Mechanical*

Engineering, *45*(2), 233-248. https://doi.org/10.1139/tcsme-2020-0035

Uematsu, Y., Tokaji, K., Tozaki, Y., Kurita, T., & Murata, S. (2008). Effect of re-filling probe hole on tensile failure and fatigue behaviour of friction stir spot welded joints in Al–Mg–Si alloy. *International Journal of Fatigue*, *30*(10-11), 1956-1966. https://doi.org/10.1016/j.ijfatigue.2008.01.006.

Van, D., Lee, S. H., Kim, K., & Sim, H. (2019). Weldability and lamellar tearing susceptibility of high-strength SN 490C steel plates. *Metals*, *9*(5), 551. https://doi.org/10.3390/met9050551

Wang, S., Zhang, Y., Wen, G., Qi, J., Zhai, W., & Gao, W. (2024). Compressive behavior and deformation mechanisms of gradient microstructures in a dissimilar welded joint. *Physica Scripta*, *99*(9), 095960. https://doi.org/10.1088/1402-4896/ad6d19

Xu, W., Wang, H., Lu, H., Liu, Y., & Dong, J. (2021). Effect of thermal exposure on microstructure and mechanical properties of friction stir welding 7B50-T7451 aluminium alloy thick plate joint. *Journal of Materials Research and Technology*, *15*, 6415-6433. https://doi.org/10.1016/j.jmrt.2021.11.082

Yu, M., Zhao, H., Zhang, Z., Zhou, L., & Song, X. (2022). Friction surfacing assisted refilled friction stir spot welding of AA6061 alloy and Q235 steel. *Journal of Manufacturing Processes*, *77*, 1-12. https://doi.org/10.1016/j.jmapro.2022.03.006

Zhang, Z.-k., & Gang, Z. (2014). Friction stir keyholeless spot welding of AZ31 Mg alloy-mild steel. *Transactions of Nonferrous Metals Society of China*, *24*(6), 1709-1716. https://doi.org/10.1016/S1003-6326(14)63244-1